New Methods for Fast Detection for Embedded Cognitive Radio

Gregoire de Broglie, Louis Morge-Rollet, Denis Le Jeune, Frédéric Le Roy, Christian Roland, Charles Canaff, Jean-Philippe Diguet

New Methods for Fast Detection for Embedded Cognitive Radio

Grégoire de Broglie*, Louis Morge-Rollet*, Denis Le Jeune*, Frédéric Le Roy*, Christian Roland†, Charles Canaff*, and Jean-Philippe Diguet‡
* ENSTA-Bretagne, Brest, France
† Université Bretagne Sud, Lorient, France
‡ IRL Crossing, Adelaide, Australia

***Abstract*—Spectrum Sensing is an important part of Cognitive Radio (CR) process. It can be used to determine if a Primary User (PU) (i.e. a licensed user) is emitting or not in the communication channel. This paper presents and compares three types of FFT-based detection algorithms for LTE-Advanced (LTE-A) cellular network at Orthogonal Frequency Division Multiple Access (OFDMA) level. These detectors sense the usage of the minimum time-frequency called Resource Block (RB). They are also low latency detectors and they only need one particular Orthogonal Frequency Division Multiplexing (OFDM) symbol to detect the usage of one RB. The three new detectors are based respectively on energy, correlation, and one what will be called *eogration* which combines energy and correlation. We analyze them with the Fisher's ratio and simulations of hypothesis test. The computing complexity of these detectors is also theoretically analyzed to provide guidance for future implementations.**

I. Introduction

A. Motivation

Cognitive Radio (CR) might be seen as improvement of the efficiency of the spectrum assignment policy as described in [1] and [2]. This will permit more accurate and adaptive emitter by quickly changing carrier frequency, bandwidth, power emission, and modulation used. It enables opportunistic or negotiated spectrum access from a Secondary User (SU) without interfering with the licensed Primary User (PU). This paper addresses the efficiency of PU's signal detection.

We will make use of the Orthogonal Frequency Division Multiple Access (OFDMA), which is mainly used in Wi-Fi (802.11ax), WiMAX, and notably by LTE-Advanced (LTE-A) cellular radio. The LTE-A allows us to do detection and non-interfering transmission operations: it is a long range communication standard compared to Wi-Fi and it defines a minimum resource for users, called the Resource Block (RB), to make scheduling easier. The RB is a two-dimensional combination of 12 subcarriers and 7 temporal symbols which are assigned by pairs to a User Equipment (UE). A pair of RBs is called subframe. This minimum resource gives us the pace to operate, but it must be done carefully to not interfere with control and synchronization data as specified in the LTE-A standard. The Fig. 1 depicts an example of LTE-A RB band where subframes can contain or not data.

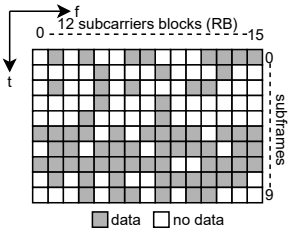

Fig. 1. Example of a LTE-A group of subframes

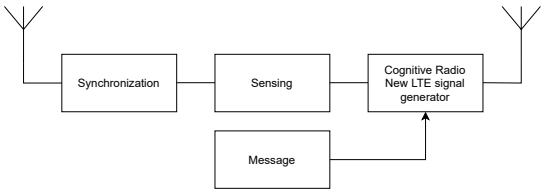

Fig. 2. Schematic diagram of the LTE-A CR network

In this study, we provide detector solutions for a LTE-A CR network where data are send in unused RBs as showed in Fig. 2. The detectors can be embedded in systems with limited payload and processing resources such as Unmanned Aerial Vehicle (UAV). After prior synchronization, these detectors will detect the availability of each subframe of the LTE-A band as shown in Fig. 1. They will consist of small, energy-efficient, low-power and low-latency computing platforms. Those communication platforms need to be autonomous from the "host" LTE-A system, so we designed them to only use the downlink synchronization signals from the Base Transceiver Station (BTS). This will also limit the knowledge of the system information of the BTS. In order to obtain low latency system, we chose to store only one temporal symbol in memory. We do precise filtering on RB to detect the LTE-A signal in a subframe. We limited the sensing time duration to one Orthogonal Frequency Division Multiplexing (OFDM) symbol. Sensing computations have to be as fast as possible to leave as much free symbols as possible for opportunistic communications. The complete frequency and time model will be shown on Section II-B.

B. Related Work

Spectrum sensing of the frequency band occupation during CR process can be carried out with many methods. We will first study one of the simplest solution: the energy detector, a useful reference to compare with. It has low computational and implementation complexities and can be used without any knowledge of the signal's characteristics. Reference [3] depicts an optimal threshold setting algorithm to minimize the error decision probability at low Signal-to-Noise Ratio (SNR) levels for different spectrum utilizations. Reference [4] presents an energy detector which uses a Welch periodogram to avoid interferences between macro and femtocells. Reference [5] describes long and short term spectrum sharing with some algorithms to detect a signal produced by the PU at the same time as the SU. It analyzes a complete LTE-A subframe and assume that the next subframe would also be free. In those conditions, an unintended transmission done by PU would be seen as interferences and detected by the CR system. Reference [6] describes a spectrum sensing algorithm that works with Welch's energy detection and discrete wavelet packet transform based energy detection. The detection probability P_d and the false alarm probability P_f are often too weak at low SNR but, as mentioned in [6]: *a higher P_d or lower P_f value can be obtained with the increase of the number of samples N or SNR*, but increasing the number of samples leads to a slower system, which means that the low latency constraint would not be respected.

The matched filter detector stated in [7] makes a cross-correlation between an unknown signal and a known copy of the expected one. This implies knowledge of the signal's parameters like modulation, code, waveform. Unfortunately, that is impossible in LTE-A in a blind acquisition mode due to the number of combinations of parameters and the usage of scrambling.

The cyclostationary detector described by [8]–[10] uses inherent periodicity to detect the presence of a signal. It is a very reliable detector which looks for periodicity of statistical properties in a cyclostationary signal. But this is inapplicable to our problem because of its heavy load of data and computing latency. Reference [11] uses a covariance matrix and the maximum eigenvalue detector but these are inoperable here because the first needs too much data and the second requires high complexity calculations which are too time expensive as we will see. Finally, the correlation detector can be a suitable solution but not as described in [12] and [13] because, they need several OFDM symbols which contradict the "one symbol" treatment used in methods considered in this paper.

Otherwise, detection of LTE-A and OFDMA signals has been explored in many ways. Reference [14] worked on Simultaneous Sensing and Transmission (SSR) and on timing alignment in CR. Reference [15] developed a detection algorithm on whole frequency bandwidth which works with or without knowledge of Cyclic Prefix (CP) length. Reference [16] is about uncertainties detection with a correlation in order to estimates the arrival time and the carrier frequency at the receiver. Reference [4] studied a LTE's signal detector working with Welch periodogram. Reference [17] proposed a methodology to do spectrum sensing and to classify the state of the primary system depending on the signal's type (control or traffic) and interfering or not with the primary system. Reference [18] worked on an RB detector with Maximum Likehood Estimate (MLE) techniques for low SNR conditions but not on streaming. So far, we talked about opportunistic systems, but there is also coordinated spectrum sensing algorithm like [19] and [20], which are more efficient than opportunistic systems and avoid hidden node problem or similar issues. We cannot use this type of sensing algorithm here because we want to develop an autonomous system which does not require to communicate with the BTS, only listen it for synchronization.

C. Contributions

In this paper, we consider and compare three new LTE-A RB signal's detectors: the energy detector, the correlator, and one that we will call "eogration". The correlator works with the 2 CPs of the same symbol, so it is different from [12], [13]. The eogration uses both energy and correlation to perform detection. The first two detectors are very classic but we propose here a new low latency implementation with a Discrete Fourier Transform (DFT) that allows RB filtering. We have to pay attention to LTE-A specifications because the standard use some carriers and symbol to transmit control and synchronization data. We also analyze which of those can be useful to create an autonomous CR system according to the constraints we fixed before.

D. Paper Organization

The rest of the paper is organized as follows. In section II, the signal's model is presented. Section III details theoretical results and simulations' detection about the three detection methods for one symbol over the whole bandwidth. We expose the adjustments and the simulations' detection for making the analyze over one RB in section IV. We do simulations of detection with a more realistic signal generator in section V. In section VI, we discuss the results obtained in the previous section and then we conclude in section VII.

II. Signal model

A. Signal model and propagation

The typical OFDM modulator used by an eNodeB (a LTE-A Base Station (BS)) in downlink communications is as follows. First, complex data $[a_0, \cdots, a_{N-1}]$ are used as an array of frequency data. They are processed by an Inverse Discrete Fourier Transform (IDFT) to obtain time domain data. The end of the symbol is then copied at the beginning to prevent intersymbol interference (ISI) produced during propagation. This step is called CP.

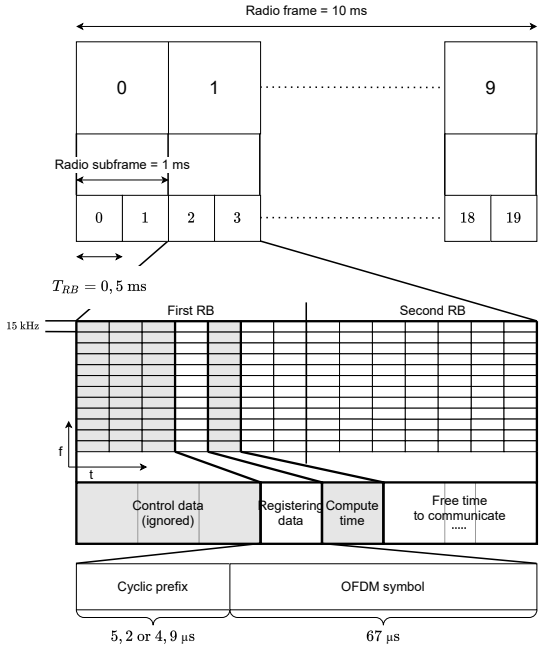

Fig. 3. Fourth generation (4G) radio frame model used in this paper

In the following, we assume non-dispersive channel. And, the OFDM signal $s[n]$ is only affected by a complex Additive White Gaussian Noise (AWGN) $w[n]$. We model each sample of the received signal $x[n]$ as follows:

$$\begin{cases} \mathcal{H}_0 : x[n] = w[n] \\ \mathcal{H}_1 : x[n] = s[n] + w[n] \end{cases} \tag{1}$$

Data $[a_0, \cdots, a_{N-1}]$ are assumed independent, so $s[n]$ is a linear combination of independent and identically distributed (iid) variables. With enough samples, we can use the central limit theorem to infer that $s[n]$ is a Gaussian process approximation with independent real and imaginary parts, as in [16]. Nevertheless, the added CP creates a correlation between some samples, so $x[n]$ is not a white process and we can benefit from it for the detection.

B. Time and frequency constraints

We use the LTE-A downlink to transmit data simultaneously to the cellular network without disturbing it. This requires us to act in compliance with the LTE-A standard, especially with control and signalization data. We need to study the time/frequency structure of a LTE-A transmission. The largest temporal unit is the frame of $10\,\mathrm{ms}$. Each frame is divided in subframe of $1\,\mathrm{ms}$ and each subframe in 2 RBs. Each RB consists of 7 time symbols, each approximately $70\,\mu\mathrm{s}$ long and 12 frequency bins. The frequency bins are spaced by $15\,\mathrm{kHz}$, so 12 bins are equal to $180\,\mathrm{kHz}$. This information is summarized in Fig. 3. As a key prerequisite, we consider that we need to be synchronized in time and in frequency to the targeted LTE-A network. This can be done with the help of Primary Synchronisation Signal (PSS) and Secondary Synchronisation Signal (SSS). These signals are transmitted on the 6 central RBs, two times by a radio frame (every $5\,\mathrm{ms}$).

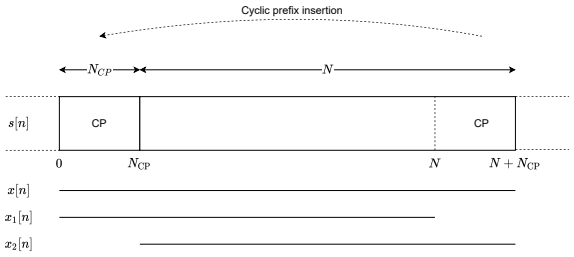

Fig. 4. Two signals model

In LTE-A, physical data can be "control" or "user" data. The first are transmitted at each subframe, i.e. every two RBs. They can occupy a variable length of at most the first 3 symbols of a subframe. The user data are transmitted on the remaining symbols of the subframe.

Under the constraint of real time processing, time is short to decode subframes' size. So, we must consider the worst possible case: control data can occupy the first 3 symbols of each subframe and user data uses the rest. Furthermore, the LTE-A standard spreads the control data over the whole band without obvious link with the corresponding user data. So, we cannot deduce the distribution of user data based on the control data. We only can be sure that the presence of user data on the 4$^{\text{th}}$ symbol lead to a presence to the end of the subframe: the next 10 symbols.

These properties led us to the following setup: we ignore the first 3 symbols, we register the 4$^{\text{th}}$ to detect if data are transmitted, the detection is done during 5$^{\text{th}}$, and if there is no user signal in the 4$^{\text{th}}$, we communicate from 6$^{\text{th}}$ to 14$^{\text{th}}$. This is also represented in Fig. 3.

III. Preliminary study: detection of one symbol

A. Introduction

Statistical hypotheses in discrete temporal domain are described in (1). With $x[n]$ the signal received and then analyzed, $s[n]$ the OFDM signal, and $w[n]$ the complex AWGN. Furthermore, we have the following probability densities: $w[n] \sim \mathcal{CN}(0, \sigma_w^2)$ and $s[n] \sim \mathcal{CN}(0, \sigma_s^2)$.

Let N be the symbol length, N_{CP} the size of the CP, and $\mathrm{rect}_N(n)$ the rectangular non-null function on $[\![-N/2, N/2]\!]$. With these notations, we can create two signals as shown on Fig. 4:

$$\begin{cases} x_1[n] = x[n]\,\mathrm{rect}_N[n - N/2] \\ x_2[n] = x[n + N_{\mathrm{CP}}]\,\mathrm{rect}_N[n - N/2] \end{cases} \tag{2}$$

In hardware implementations, we consider that the entire OFDM symbol $x[n]$ on Fig. 4 is stored before the calculation. This suppose that the detector is synchronized with the eNodeB as said in II-B.

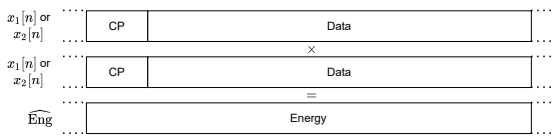

Fig. 5. Working principle of energy estimator

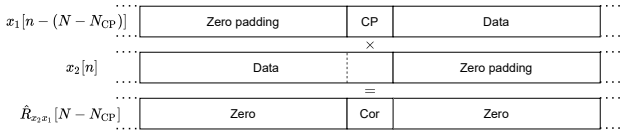

Fig. 6. Working principle of correlation estimator

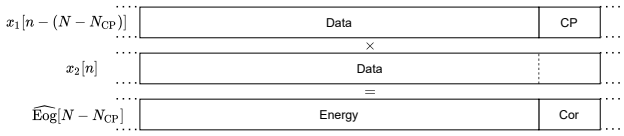

Fig. 7. Working principle of eogration estimator

The emitted signal $s[n]$ is an OFDM signal modulated with an IDFT. So, the estimators use DFT and IDFT to do computations in frequency domain and for filtering the symbol $x[n]$ analyzed.

We have two hypotheses that correspond to two classes. We have also three estimators and we want to select the best, i.e. the one that separates as much as possible the two classes. We need a metric for that and we choose the Fisher's ratio [21]. [22] used it in a similar situation, and the ratio takes account of the between-class variance and the within-class variance. The ratio is defined as follows:

$$F = \frac{\left(\mu_{\mathcal{H}_0} - \mu_{\mathcal{H}_1}\right)^2}{\sigma^2_{\mathcal{H}_0} + \sigma^2_{\mathcal{H}_1}} \tag{3}$$

with $\mu_{\mathcal{H}_0}$ and $\sigma^2_{\mathcal{H}_0}$ the expected value and variance for null hypothesis ($\mathcal{H}_0$) and, $\mu_{\mathcal{H}_1}$ and $\sigma^2_{\mathcal{H}_1}$ the expected value and variance for alternative hypothesis ($\mathcal{H}_1$).

B. Energy estimator

We present here the energy estimator we have developed. The canonical formula of an energy estimator is the following: $\sum_{n=0}^{N-1} |x[n]|^2 = \sum_{n=0}^{N-1} x[n] \times x^*[n]$. We compute here the energy of an OFDM symbol and we do this in the frequency domain to allow the filtering of the RB. This is made possible by the Parseval's identity. The OFDM's properties are retained by doing the filtering with DFT and IDFT of the same length as the OFDM modulator in the eNodeB: N samples. So, we select for this calculus one of the two signals: $x_1[n]$ or $x_2[n]$, they are equivalent here because they contains the same amount of information: a complete OFDM symbol of N samples. This is why we have "$x_1[n]$ or $x_2[n]$" at the left of the Fig. 5 which describes the working principle of the energy estimator. The statistical properties of the latter are showed in Table I.

$$\widehat{\text{Eng}}[m] = \underset{N \text{ points}}{\text{IDFT}}\left\{ \underset{N \text{ points}}{\text{DFT}}\{x_1\} \times \underset{N \text{ points}}{\text{DFT}}\{x_1\}^* \right\} \tag{4}$$

$$\widehat{\text{Eng}}[m] = \frac{1}{N}\sum_{n=0}^{N-1}\left(\sum_{k=0}^{N-1} x_1[k]e^{-2j\pi\frac{kn}{N}}\right) \left(\sum_{l=0}^{N-1} x_1[l]e^{-2j\pi\frac{ln}{N}}\right)^* e^{2j\pi\frac{nm}{N}} \tag{5}$$

$$\widehat{\text{Eng}}[m=0] = \sum_{k=0}^{N-1} |x[k]|^2 \tag{6}$$

C. Correlation estimator

We also developed a correlation estimator showed in Fig. 6. As in III-B, it does the compute in frequency domain to allow RB filtering (but here with $2N$ points and a zero padding). The correlation classic formula is $R_{xy}[\tau] = \sum_{n=0}^{N-1} x[n+\tau]y^*[n]$ in temporal domain and $R_{xy}[f] = X[f]Y^*[f]$ in frequency domain. The output of the correlation estimator is about the CP because it is the only repeated part in the complete symbol $x[n]$ in Fig. 4. The statistics of this estimator are also in Table I.

$$\widehat{R}_{x_2x_1}[m] = \underset{2N \text{ points}}{\text{IDFT}}\left\{ \underset{2N \text{ points}}{\text{DFT}}\{x_2\} \times \underset{2N \text{ points}}{\text{DFT}}\{x_1\}^* \right\} \tag{7}$$

$$\widehat{R}_{x_2x_1}[m] = \frac{1}{2N}\sum_{n=0}^{2N-1}\left(\sum_{k=0}^{2N-1} x_2[k]e^{-2j\pi\frac{kn}{2N}}\right) \left(\sum_{l=0}^{2N-1} x_1[l]e^{-2j\pi\frac{ln}{2N}}\right)^* e^{2j\pi\frac{nm}{2N}} \tag{8}$$

$$\widehat{R}_{x_2x_1}[m = N - N_{\text{CP}}] = \sum_{l=0}^{N_{\text{CP}}-1} x[l+N]x^*[l] \tag{9}$$

D. Eogration estimator

The eogration estimator is a detector which is working in frequency domain like the others to permit RB filtering. The frequency product of the circularly rotated conjugated signal x_1 and the signal x_2 as described in Fig. 7 gives us a result divided in two parts: the energy over the data part and the correlation over the CP part. The statistics of the eogration are also in Table I.

$$\widehat{\text{Eog}}[m] = \underset{N \text{ points}}{\text{IDFT}}\left\{ \underset{N \text{ points}}{\text{DFT}}\{x_2\} \times \underset{N \text{ points}}{\text{DFT}}\{x_1\}^* \right\} \tag{10}$$

$$\widehat{\text{Eog}}[m] = \frac{1}{N}\sum_{n=0}^{N-1}\left(\sum_{k=0}^{N-1} x_2[k]e^{-2j\pi\frac{kn}{N}}\right) \left(\sum_{l=0}^{N-1} x_1[l]e^{-2j\pi\frac{ln}{N}}\right)^* e^{2j\pi\frac{nm}{N}} \tag{11}$$

Table I
STATISTICS OF THE ESTIMATORS

		$\widehat{\text{Eng}}$	$\widehat{R}_{x_2x_1}$	$\widehat{\text{Eog}}$
$\mathcal{H}_0$	$\mathbb{E}$	$N\sigma_w^2$	0	$(N-N_{\text{CP}})\sigma_w^2$
	Var	$N(\sigma_w^2)^2$	$N_{\text{CP}}(\sigma_w^2)^2$	$N(\sigma_w^2)^2$
$\mathcal{H}_1$	$\mathbb{E}$	$N(\sigma_s^2+\sigma_w^2)$	$N_{\text{CP}}\sigma_s^2$	$N_{\text{CP}}\sigma_s^2+(N-N_{\text{CP}})(\sigma_s^2+\sigma_w^2)$
	Var	$N(\sigma_s^2+\sigma_w^2)^2$	$N_{\text{CP}}(\sigma_s^2+\sigma_w^2)^2$	$N(\sigma_s^2+\sigma_w^2)^2$
Fisher ratio		$N\frac{(\sigma_s^2)^2}{(\sigma_w^2)^2+(\sigma_s^2+\sigma_w^2)^2}$	$N_{\text{CP}}\frac{(\sigma_s^2)^2}{(\sigma_w^2)^2+(\sigma_s^2+\sigma_w^2)^2}$	$N\frac{(\sigma_s^2)^2}{(\sigma_w^2)^2+(\sigma_s^2+\sigma_w^2)^2}$

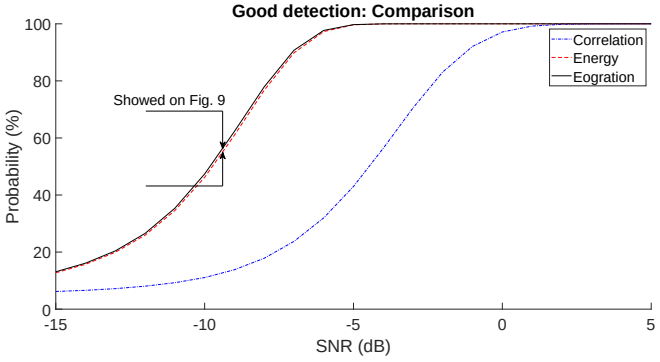

Fig. 8. Good detection performance for a false alarm rate of 0.05

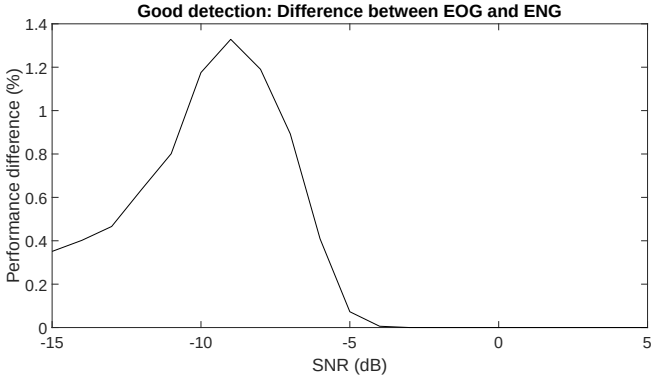

Fig. 9. Difference of performance detection between energy and eogration estimator

$$\widehat{\text{Eog}}[m=N-N_{\text{CP}}]=\sum_{l=0}^{N_{\text{CP}}-1}x[l+N]x^*[l]+\sum_{l=N_{\text{CP}}}^{N-1}|x[l]|^2 \tag{12}$$

The details of all calculations are showed in appendix A. Only the eogration is described because it is made of an energy and a correlation estimators.

E. Comparison of Fisher's ratios

Table I shows the statistics of the three estimators. The Fisher's ratios of the three estimators are equal at one exception: the multiplier. Indeed, the multiplier is N_{CP} for the correlator and N for the others. In LTE-A, $N_{\text{CP}} \approx 0.07 \times N$. So the Fisher's ratio of the correlation is too small compare to the Fisher's ratios of energy and eogration. The ratios of eogration and energy are equals because both got the same variance and eogration's expected value is within a constant ($-N_{\text{CP}}\sigma_w^2$), the same as energy making their difference equal. We also add that the Fisher's ratio does not take care of many characteristics of probability density like its skewness. So, identical Fisher's ratios do not necessarily imply identical performances, but it is a good indicator for the first step of a performances' comparison, before detection simulations.

F. Simulations

Signal generated by an OFDM process approximates a complex Gaussian process [16] and the noise in our model is an AWGN. The signals $s[n]$ and $w[n]$ are generated as Gaussian processes. Then, we create the CP for $s[n]$. According to the typical configuration for a 4G bandwidth of 3 MHz, the symbol length used is $N = 256$ and $N_{\text{CP}} = 18$.

We simulate two configurations $\mathcal{H}_0$ and $\mathcal{H}_1$ with 10 000 trials. We make an hypothesis test by setting the false alarm rate as 5 %. For this, we set the threshold as 95 % of the value of $\mathcal{H}_0$ hypothesis, which let 5 % of error. For $\mathcal{H}_1$, we set the noise power σ_w^2 to 1 and modify the signal power σ_s^2 accordingly to SNR value. Finally, we plot the good detection probability $\mathbb{P}(\hat{\mathcal{H}}_1|\mathcal{H}_1)$ in Fig. 8 with a false alarm probability of $\mathbb{P}(\hat{\mathcal{H}}_1|\mathcal{H}_0) = 0.05$.

G. Selection of good detectors

We saw that energy and eogration estimators got greater Fisher's ratio than the correlation due to the fact that they are proportional to N and N_{CP} respectively with $N > N_{\text{CP}}$. Moreover, we can see in Fig. 8 that the correlator is far less effective than the others. So, we chose to reject the correlation estimator. Concerning energy and eogration estimators, the performances of eogration are slightly better for the simulations than energy estimator ones and it depends on CP length, as we can see, for one RB, in Fig. 14. The performance's differences between them for the whole band are shown in Fig. 9.

IV. RB DETECTOR'S APPLICATION

A. RB filtering

We seek to detect the usage of an OFDM symbol over one RB, i.e. 12 subcarriers among all. The frequency bins are all independents, so we can subtract the useless ones by setting their values to 0 in frequency domain. The Fast Fourier Transform (FFT) and Inverse Fast Fourier Transform

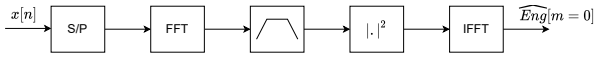

Fig. 10. Block diagram of the energy estimator

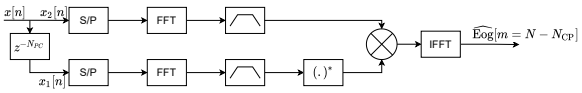

Fig. 11. Block diagram of the eogration estimator

Table II
TABLE OF COMPUTE COMPLEXITY FOR A RB OF 12 SUBCARRIERS

Operator name	multiplier	adder	inverter
FFT & IFFT	$N/2 \log_2 N$	$N \log_2 N$	0
$\|\ \|^2$	12	0	12
$(\ )^*$	0	0	12
multiplier operator	12	0	0
Eogration	$3N/2 \log_2(N) + 12$	$3N \log_2(N)$	12
Eogration ($N = 1024$)	15 372	30 720	12
Energy	$N \log_2(N) + 12$	$2N \log_2(N)$	12
Energy ($N = 1024$)	10 252	20 480	12

(IFFT) used to do this use a rectangular windows function because of nature of OFDM. Indeed, the bins of the OFDM are frequency spaced by the roots of sinc function, which makes them orthogonal in pairs.

B. Detector architectures

We present here the two schemes of the energy and eogration estimators in Fig. 10 and 11. The sign of the delay is negative in the block diagram and became positive in the mathematical model, because one describes the data recording whereas the other process the data already registered, so we can use the $+$ sign and stay deterministic. We can see the complexity gap between the estimators, the eogration needs much more computations on two parallel processes to obtain results.

We consider three computing units for the analysis of the computational complexity of the two detectors: the complex multiplier, the complex adder, and the inverter. The Table II is about computational complexity of each block of the Fig. 10 and Fig. 11. We consider the computation load for a RB detection (12 subcarriers) we give the results too for a typical value $N = 1024$.

C. Simulations of RB detection

Simulations of detection over a RB subband in Fig. 12 show us lower detection performance. For example, the $80\,\%$ threshold is reached at $-8\,\mathrm{dB}$ in Fig. 8 and at $0\,\mathrm{dB}$ in Fig. 12. This drop is perfectly understandable because we massively reduced the number of available data.

V. SIMULATIONS WITH A LTE-A SIGNAL GENERATOR

To confirm our detection performances, we made a signal generator by complying with respect to a part of the 4G

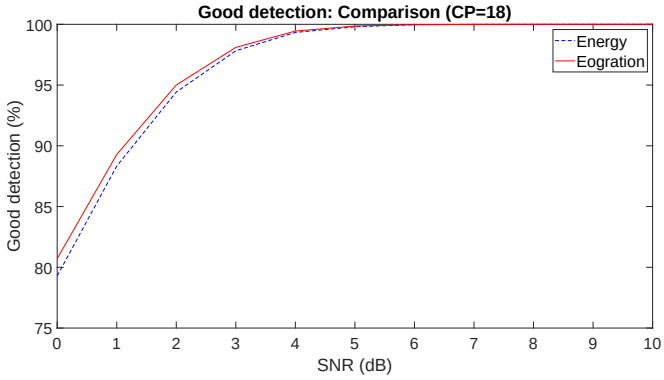

Fig. 12. Estimator comparison for a CP of 18 samples, a symbol of 256 samples, and on a RB subband

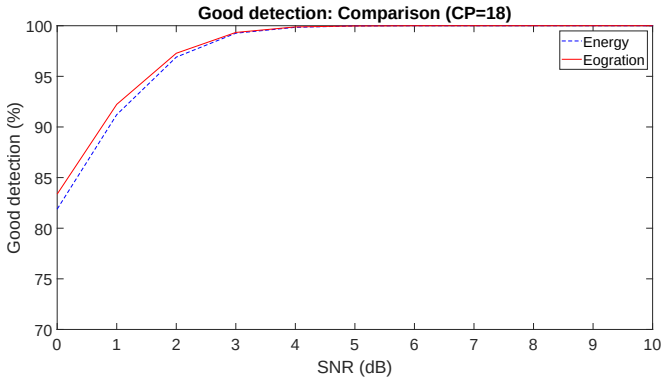

Fig. 13. Estimator comparison for a CP of 18 samples on a 15 RBs subband with a more realistic model

standard: the frequency sampling of the generator varies between $1.92\,\mathrm{MHz}$, $3.84\,\mathrm{MHz}$, $7.68\,\mathrm{MHz}$, $15.36\,\mathrm{MHz}$, and $30.72\,\mathrm{MHz}$ which correspond to 6 RBs, 15 RBs, 25 RBs, 50 RBs, 75 RBs, and 100 RBs respectively (the last two are sampled at $30.72\,\mathrm{MHz}$); the FFT length changes between 128 and 2048, the guardband and the CP length are specified in [23], and modulations used here are Quadrature Phase Shift-Keying (QPSK), 16-Quadrature Amplitude Modulation (QAM) and 64-QAM. Results are shown in Figure 13. They are similar to those of the earlier section, which is an information about the reliability of the model used and the results.

VI. DISCUSSION

It can be seen that the detection performances of the eogration detector may change with the length of the CP. As shown in Fig. 14, we can see a discrepancy in performance between the energy detector and the one with eogration at SNR between $-20\,\mathrm{dB}$ to $5\,\mathrm{dB}$.

These two detectors will led us to a trade-off because the energy estimator is slightly less efficient than the eogration estimator with a one third less complex implementation. So, it is an advantage for an embedded system which does not have access to a powerful computing platform.

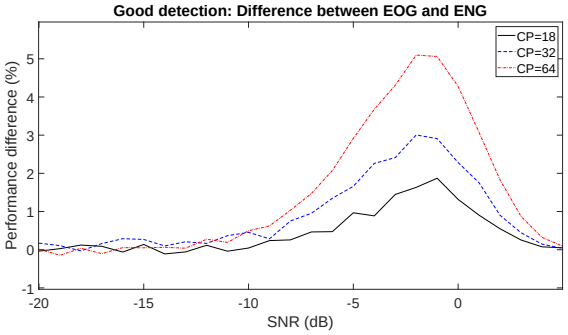

Fig. 14. Difference of performance detection between energy and eogration for multiple CP length

VII. Conclusion

We developed in this paper three new detectors for RB analysis of LTE-A Downlink (DL) signal. They work respectively with energy, correlation and eogration. We used the Fisher's ratio and detection statistics to show their usability. We also exhibit that the eogration estimator is slightly better than the energy estimator in Fig. 8 and Fig. 14, despite a computational complexity which is one and half times greater than the complexity of energy detection. This difference will be less important in the future because the estimators do not need costly math function and the number of computing units is low for state of the art calculators. We can therefore assume that the eogration estimator could be the default choice in the future. Most of the difficulties for the implementation comes from the real-time constraint of 30 µs on the detection. The remaining of the 70 µs will be used to prepare our own data to be emitted.

Appendix A
Detailed computations of the eogration

We compute here the eogration estimator described in Fig. 7 (x_1's data are circularly rotated so, the end of the signal goes to the beginning):

$$\widehat{\mathrm{Eog}}[m] = \frac{1}{N}\sum_{n=0}^{N-1}\left(\sum_{k=0}^{N-1} x_2[k]e^{-2j\pi\frac{kn}{N}}\right)\left(\sum_{l=0}^{N-1} x_1[l]e^{-2j\pi\frac{ln}{N}}\right)^* e^{2j\pi\frac{nm}{N}} \tag{13}$$

$$\widehat{\mathrm{Eog}}[m] = \sum_{k=0}^{N-1}\sum_{l=0}^{N-1} x_2[k]x_1^*[l]\left(\frac{1}{N}\sum_{n=0}^{N-1} e^{-2j\pi\frac{((k-l)-m)n}{N}}\right) \tag{14}$$

We are interested by estimating $\widehat{\mathrm{Eog}}[m = N - N_{\mathrm{CP}}]$, so the mean sum of exponentials is equal to 1 if $k - l = N - N_{\mathrm{CP}}$ or when $k - l = -N_{\mathrm{CP}}$. So, for $k = l + (N - N_{\mathrm{CP}})$, we have:

$$\widehat{\mathrm{Eog}}[m = N - N_{\mathrm{CP}}] = \sum_{k=0}^{N-1}\sum_{l=0}^{N-1} x_2[k]x_1^*[l]\,\delta[(k-l) - (N - N_{\mathrm{CP}})] \tag{15}$$

$$= \sum_{k=0}^{N-1} x_2[l + (N - N_{\mathrm{CP}})]x_1^*[l] \tag{16}$$

$$= \sum_{l=0}^{N_{\mathrm{CP}}-1} x_2[l + (N - N_{\mathrm{CP}})]x_1^*[l] \tag{17}$$

$$= \sum_{l=0}^{N_{\mathrm{CP}}-1} x[l + N]x^*[l] \tag{18}$$

For $k = l - N_{\mathrm{CP}}$, we have:

$$\widehat{\mathrm{Eog}}[m = N - N_{\mathrm{CP}}] = \sum_{k=0}^{N-1}\sum_{l=0}^{N-1} x_2[k]x_1^*[l]\,\delta[(k-l) - (N - N_{\mathrm{CP}}) + N] \tag{19}$$

$$= \sum_{l=0}^{N-1} x_2[l - N_{\mathrm{CP}}]x_1^*[l] \tag{20}$$

$$= \sum_{l=N_{\mathrm{CP}}}^{N-1} x_2[l - N_{\mathrm{CP}}]x_1^*[l] \tag{21}$$

$$= \sum_{l=N_{\mathrm{CP}}}^{N-1} |x[l]|^2 \tag{22}$$

So, we obtain the following estimator:

$$\widehat{\mathrm{Eog}}[m = N - N_{\mathrm{CP}}] = \sum_{l=0}^{N_{\mathrm{CP}}-1} x[l + N]x^*[l] + \sum_{l=N_{\mathrm{CP}}}^{N-1} |x[l]|^2 \tag{23}$$

Now, we want to find the associated statistical properties. We begin by the energy part of the eogration: $\sum_{l=N_{\mathrm{CP}}}^{N-1} |x[l]|^2$. We have for $\mathcal{H}_0$: $x[n] \sim \mathcal{CN}(0, \sigma_w^2)$ and for $\mathcal{H}_1$: $x[n] \sim \mathcal{CN}(0, \sigma_w^2 + \sigma_s^2)$. We know in [24] that $|x[n]|^2$ become an exponential law with a parameter λ equal to $1/\sigma_w^2$ or $1/(\sigma_s^2 + \sigma_w^2)$ depending on the hypothesis. So, the expected value and the variance are:

$$\mathcal{H}_0 \begin{cases} \mathbb{E}\left(\sum_{n=0}^{N-1} |x[n]|^2\right) & = N\sigma_w^2 \\ \mathrm{Var}\left(\sum_{n=0}^{N-1} |x[n]|^2\right) & = N(\sigma_w^2)^2 \end{cases} \tag{24}$$

$$\mathcal{H}_1 \begin{cases} \mathbb{E}\left(\sum_{n=0}^{N-1} |x[n]|^2\right) & = N(\sigma_s^2 + \sigma_w^2) \\ \mathrm{Var}\left(\sum_{n=0}^{N-1} |x[n]|^2\right) & = N(\sigma_s^2 + \sigma_w^2)^2 \end{cases} \tag{25}$$

The calculations for the correlation part are quite different. The variance formula with a complex random variables is the following:

$$\mathrm{Var}(Z) = E\left[|Z - E[Z]|^2\right] \tag{26}$$

$$\mathrm{Var}(Z) = E\left[|Z|^2\right] - |E[Z]|^2 \tag{27}$$

and the formula of the variance for complex and independent random variables is:

$$\begin{aligned}\mathrm{Var}(XY) = &\mathrm{Var}(X)\,\mathrm{Var}(Y) \\ &+ \mathrm{Var}(X)|E[Y]|^2 \\ &+ \mathrm{Var}(Y)|E[X]|^2\end{aligned} \tag{28}$$

So we obtain the following statistics:

$$\mathcal{H}_0 \begin{cases} \mathbb{E}\left(\widehat{R}_{x_2x_1}\right) & = 0 \\ \mathrm{Var}\left(\widehat{R}_{x_2x_1}\right) & = N_{\mathrm{CP}}(\sigma_w^2)^2 \end{cases} \tag{29}$$

$$\mathcal{H}_1 \begin{cases} \mathbb{E}\left(\widehat{R}_{x_2x_1}\right) & = N_{\mathrm{CP}}\sigma_s^2 \\ \mathrm{Var}\left(\widehat{R}_{x_2x_1}\right) & = N_{\mathrm{CP}}(\sigma_s^2+\sigma_w^2)^2 \end{cases} \tag{30}$$

Finally, since the eogration is a sum of a correlation and an energy, the statistics are:

$$\mathcal{H}_0 \begin{cases} \mathbb{E}\left(\widehat{\mathrm{Eog}}\right) & = (N-N_{\mathrm{CP}})\sigma_w^2 \\ \mathrm{Var}\left(\widehat{\mathrm{Eog}}\right) & = N(\sigma_w^2)^2 \end{cases} \tag{31}$$

$$\mathcal{H}_1 \begin{cases} \mathbb{E}\left(\widehat{\mathrm{Eog}}\right) & = N_{\mathrm{CP}}\sigma_s^2 + (N-N_{\mathrm{CP}})(\sigma_s^2+\sigma_w^2) \\ \mathrm{Var}\left(\widehat{\mathrm{Eog}}\right) & = N(\sigma_s^2+\sigma_w^2)^2 \end{cases} \tag{32}$$

REFERENCES

[1] J. Mitola and G. Maguire, "Cognitive radio: Making software radios more personal," *IEEE Pers. Commun.*, vol. 6, no. 4, pp. 13–18, Aug./1999.

[2] H.-s. Chen, W. Gao, and D. G. Daut, "Spectrum sensing for OFDM systems employing pilot tones," *IEEE Transactions on Wireless Communications*, vol. 8, no. 12, pp. 5862–5870, Dec. 2009.

[3] N. Wang and Y. Gao, "Optimal Threshold of Welch's Periodogram for Sensing OFDM Signals at Low SNR Levels," in *European Wireless 2013; 19th European Wireless Conference*, Apr. 2013, pp. 1–5.

[4] I. Harjula and A. Hekkala, "Spectrum sensing in cognitive femto base stations using welch periodogram," in *2011 IEEE 22nd International Symposium on Personal, Indoor and Mobile Radio Communications*. Toronto, ON, Canada: IEEE, Sep. 2011, pp. 2305–2309.

[5] P. Karunakaran, T. Wagner, A. Scherb, and W. Gerstacker, "Sensing for Spectrum Sharing in Cognitive LTE-A Cellular Networks," *arXiv:1401.8226 [cs, math]*, Jan. 2014.

[6] N. Wang, Y. Gao, F. Yang, Q. Bi, W. Xie, and C. Parini, "Energy detection-based spectrum sensing with constraint region in cognitive LTE systems," *Transactions on Emerging Telecommunications Technologies*, vol. 28, no. 11, p. e3171, 2017.

[7] A. E. Omer, "Review of spectrum sensing techniques in Cognitive Radio networks," in *2015 International Conference on Computing, Control, Networking, Electronics and Embedded Systems Engineering (ICCNEEE)*, Sep. 2015, pp. 439–446.

[8] O. Ali, F. Nasir, and A. A. Tahir, "Analysis of OFDM parameters using Cyclostationary spectrum sensing in cognitive radio," in *2011 IEEE 14th International Multitopic Conference*, Dec. 2011, pp. 301–305.

[9] G. Prema and P. Gayatri, "Blind spectrum sensing method for OFDM signal detection in Cognitive Radio communications," in *2014 International Conference on Communication and Network Technologies*, Dec. 2014, pp. 42–47.

[10] S. H. Sohn, N. Han, J. M. Kim, and J. W. Kim, "OFDM Signal Sensing Method Based on Cyclostationary Detection," in *2007 2nd International Conference on Cognitive Radio Oriented Wireless Networks and Communications*, Aug. 2007, pp. 63–68.

[11] W. Pan, H. Wang, and L. Shen, "Covariance matrix based spectrum sensing for OFDM based cognitive radio," in *2012 International Conference on Systems and Informatics (ICSAI2012)*, May 2012, pp. 1426–1430.

[12] H.-S. Chen, W. Gao, and D. G. Daut, "Spectrum Sensing for OFDM Systems Employing Pilot Tones and Application to DVB-T OFDM," in *2008 IEEE International Conference on Communications*, May 2008, pp. 3421–3426.

[13] A. Temtam and D. C. Popescu, "Using OFDM pilot tones for spectrum sensing with applications to mobile WiMAX," in *2014 IEEE Radio and Wireless Symposium (RWS)*, Jan. 2014, pp. 232–234.

[14] P. Karunakaran and W. H. Gerstacker, "Sensing Algorithms and Protocol for Simultaneous Sensing and Reception-Based Cognitive D2D Communications in LTE-A Systems," *IEEE Trans. Cogn. Commun. Netw.*, vol. 4, no. 1, pp. 93–107, Mar. 2018.

[15] S. Chaudhari, V. Koivunen, and H. V. Poor, "Autocorrelation-Based Decentralized Sequential Detection of OFDM Signals in Cognitive Radios," *IEEE Transactions on Signal Processing*, vol. 57, no. 7, pp. 2690–2700, Jul. 2009.

[16] J. van de Beek, M. Sandell, and P. Borjesson, "ML estimation of time and frequency offset in OFDM systems," *IEEE Trans. Signal Process.*, vol. 45, no. 7, pp. 1800–1805, Jul. 1997.

[17] S.-Y. Tu, K.-C. Chen, and R. Prasad, "Spectrum Sensing of OFDMA Systems for Cognitive Radio Networks," *IEEE Transactions on Vehicular Technology*, vol. 58, no. 7, pp. 3410–3425, Sep. 2009.

[18] Y. M. Ali, A. Ahmed, and T. Mumtaz, "Machine Learning for Improved Resource Block Detection in 4G LTE Cognitive Radio Networks," in *2021 International Mobile, Intelligent, and Ubiquitous Computing Conference (MIUCC)*, May 2021, pp. 169–175.

[19] R. Xu, M. Chen, J. Zhang, H. Wang, and W. Yu, "Report the sensing results using OFDMA in cooperative spectrum sensing," in *2010 International Conference on Wireless Communications Signal Processing (WCSP)*, Oct. 2010, pp. 1–6.

[20] G. Kokabian and A. Esmailpour, "Cooperative spectrum sensing in LTE networks," in *2014 IEEE 27th Canadian Conference on Electrical and Computer Engineering (CCECE)*, May 2014, pp. 1–5.

[21] C. Li and B. Wang, "Fisher Linear Discriminant Analysis," *CCIS Northeastern University*, p. 6, 2014.

[22] J. Zarka, F. Guth, and S. Mallat, "Separation and Concentration in Deep Networks," *arXiv:2012.10424 [cs]*, Mar. 2021.

[23] "Specification # 36.104," https://portal.3gpp.org/desktopmodules/Specifications/SpecificationDetails.aspx?specificationId=2412.

[24] A. Papoulis and S. U. Pillai, *Probability, Random Variables and Stochastic Processes*, 4th ed. McGraw-Hill, 2002, démonstrations p 190.